

We are IntechOpen, the world's leading publisher of Open Access books Built by scientists, for scientists

6,900

Open access books available

186,000

International authors and editors

200M

Downloads

Our authors are among the

154

Countries delivered to

TOP 1%

most cited scientists

12.2%

Contributors from top 500 universities



WEB OF SCIENCE™

Selection of our books indexed in the Book Citation Index
in Web of Science™ Core Collection (BKCI)

Interested in publishing with us?
Contact book.department@intechopen.com

Numbers displayed above are based on latest data collected.
For more information visit www.intechopen.com



Physics Behind the Ohmic Nature in Silicon Carbide Contacts

Zhongchang Wang

Additional information is available at the end of the chapter

<http://dx.doi.org/10.5772/50767>

1. Introduction

One of the most active fields in semiconductor research is the development of electronic devices capable of function at high power and high frequency levels, high temperatures, and caustic circumstances. This surge of activity is strongly driven by the urgent desire for replacing the current Si- and GaAs-based electronics because they are unable to operate properly under harsh environmental conditions. As a promising substitute, the wide-band-gap semiconductor, silicon carbide (SiC), has captured considerable attention recently due to its excellent intrinsic properties, which involve large breakdown electric field, high electron saturation drift velocity, strong hardness, and good thermal conductivity. On the other hand, current significant improvements in the epitaxial and bulk crystal growth of SiC have paved the way for fabricating its electronic devices, which stimulates further interest in developing device processing techniques so as to take full advantage of its superior inherent properties.

One of the most critical issues currently limiting the device processing is the manufacturing of reliable and low-resistance Ohmic contacts especially contacts to *p*-type 4H-SiC [1]. The Ohmic contacts are primarily important in SiC devices because a Schottky barrier of high energy is inclined to form at an interface between metal and wide-band-gap semiconductor, which consequently results in low current driving, slow switching speed, and increased power dissipation. Much of effort expended to date to realize the Ohmic contact has mainly focused on two techniques. One is the high-dose ion implantation approach [2], which can increase carrier density in SiC noticeably while reducing its depletion width significantly so that increasing tunneling current is able to flow across the barrier region. The key problem of this method is the easy formation of lattice defects or amorphization during the ion implantation. These defects are unfortunately very stable and need to be recovered via anneal-

ing at an extremely high temperature of about 2000 K, thereby complicating the mass production of SiC devices.

The other alternative is to generate an intermediate semiconductor layer with narrower band gap or higher carrier density at the contacts/SiC interface via depositing and annealing technique [3]. To form such layers, a wide range of materials have been examined in a trial-and-error designing fashion, including metals, silicides, carbides, nitrides, and graphite. Of all these materials, the metallic alloys have been investigated extensively, largely because their fabrication process is simple, standard, and requires no exotic materials. In particular, most of research activities have been focused on TiAl-based alloys, the only currently available materials that yield significantly low contact resistance (Ohmic contact) to *p*-SiC [4]. Moreover, they demonstrate high thermal stability. Although a lot of intriguing results have been obtained regarding the TiAl-based contact systems, the mechanism whereby the Schottky becomes Ohmic after annealing has not been well clarified yet. In other words, the key factor to understanding the formation origin of Ohmic contact remains controversial. Mohny et al. [5] proposed that a high density of surface pits and spikes underneath the contacts contributes to the formation of Ohmic behavior based on their observations using scanning electron microscopy and atomic force microscopy. Nakatsuka et al. [6], however, concluded that the Al concentration in the TiAl alloy is important for the contact formation. Using the liquid etch and ion milling techniques, John and Capano [7] ruled out these possibilities and claimed that what matters in realizing the Ohmic character is the generation of carbides, Ti_3SiC_2 and Al_4C_3 , between the metals and semiconductor. This, however, differs, to some extent, from the X-ray diffraction (XRD) findings of Chang et al. [8] showing that the compounds formed at the metal/SiC interface are silicides, TiSi_2 , TiSi , and Ti_3SiC_2 . In addition, Ohyanagi et al. [9] argued that carbon exists at the contacts/SiC interface and might play a crucial role in lowering Schottky barrier. These are just a few representative examples illustrating the obvious discrepancies in clarifying the formation mechanism of the Ohmic contact. Taking the amount of speculations on the mechanism and the increasing needs for better device design and performance control, understanding the underlying formation origin is timely and relevant.

To develop an understanding of the origin in such a complex system, it is important to focus first on microstructure characterization. Transmission electron microscopy (TEM) studies by Tsukimoto et al. [10] have provided useful information in this aspect. They have found that the majority of compounds generated on the surface of 4H-SiC substrate after annealing consist of Ti_3SiC_2 and hence proposed that the SiC/ Ti_3SiC_2 interface is responsible for the lowering of Schottky barrier in the TiAl-based contact system. However, the role of this interface in realizing the Ohmic nature is still unclear. It is not even clear how the two materials atomically bond together from their experiments, which is very important because it may strongly affect physical properties of the system. Theoretically, we have calculated the atomic structures, adhesive energies, and bonding nature of the SiC/ Ti_3SiC_2 interface [11]. However, this calculation does not actually reveal the formation mechanism of Ohmic contact because it only addresses the interface structure. Furthermore, lacking essential experimental information about the interfacial atomic-scale structure, such calculations have been incomplete.

Recent advances in the high-angle annular-dark-field (HAADF) microscopy [12,13], the highest resolution, have enabled atomic-scale imaging of a buried interface. However, direct interpretation of the observed HAADF images is not always straightforward because there might be abrupt structural discontinuity, mixing of several species of elements on individual atomic columns, or missing contrasts of light elements. One possible way out to complement the microscopic data is through atomistic calculation, especially the first-principles calculation. As well known, the atomistic first-principles simulations have long been confirmed to be able to suggest plausible structures, elucidate the reason behind the observed images, and even provide a *quantitative* insight into how interface governs properties of materials [14,15]. Consequently, a combination of the state-of-the-art microscopy and accurate atomistic modeling [16] is an important advance for determining interface atomic-scale structure and relating it to device properties, revealing, in this way, physics origin of the contact issues in SiC electronics.

In addition to determining atomic structure of the 4H-SiC/Ti₃SiC₂ interface, the goal of this work is to clarify the formation mechanism of the TiAl-based Ohmic contacts so as to provide suggestions for further improvement of the contacts. 4H-SiC will hereafter be referred to as SiC. In this Chapter, we will first attribute qualitatively the formation of ohmic contacts in the TiAl-deposited SiC system to an epitaxial and atomically abrupt interface between the SiC and Ti₃SiC₂ generated *via* annealing. The interface presumably serves as a primary current-transport pathway to lower the Schottky barrier formed at the interface between the deposited metals and SiC. Further quantitative studies reveal that the barrier mitigation arises from trapping of an atomic layer of carbon at the SiC/Ti₃SiC₂ interface, which assists the electron transport across the SiC [17,18]. The considerations on the role played by interface do not, however, exclude another possibility that the Ti₃SiC₂ atomic layers can be generated inside the SiC bulk interiors, which presents a behavior that may differ from that of their bulk [19]. Combining the state-of-the-art TEM with atomistic first-principles calculations, we demonstrate the presence of an atomic-scale Ti₃SiC₂-like bilayer embedded in the SiC, forming an atomically ordered multilayer that exhibits an unexpected electronic state with point Fermi surface. The valence charge is confined to a large extent to within the bilayer in a spatially connected manner, serving possibly as a conducting channel to enhance the current flow over the semiconductor. Further investigation into the contact regions unveils another new opportunity to allow the electron transport across the semiconductor, namely, *via* the terraces formed at the SiC/Ti₃SiC₂ interface [20]. Experimentally, the formed carbide Ti₃SiC₂ is demonstrated to bond directly to the silicon carbide at the terraces in an epitaxial and atomically ordered fashion, regardless of dimension of the terraces. There appear pronounced gap states at Fermi level in the semiconductor layers around the terraces, and charges are accumulated heavily around the terraces in a connected and broadly distributed manner. The presence of the metallicity and the likelihood to act as electron conduction channels to enable the current flow over the semiconductor make the terraces at the interface one of the origins underlying the ohmic contact in silicon carbide electronics. We therefore demonstrate in this chapter that origin of the long-standing contact issue in SiC devices can be understood and technologically manipulated at the atomic level, and suggest the key physical factors for establishing the ohmic nature.

2. Role of coherent SiC/Ti₃SiC₂ interface

The *p*-type 4H-SiC epitaxial layers (5- μm thick) doped with aluminum ($N_A = 4.5 \times 10^{18} \text{ cm}^{-3}$) which were grown on undoped 4H-SiC wafers by chemical vapor deposition (manufactured by Cree Research, Inc.) were used as substrates. The 4H-SiC substrates had 8°-off Si-terminated (0001) surfaces inclined toward a $[\bar{2}110]$ direction because only 4H-type structure of SiC with polymorph (e.g. 3C, 4H, 6H, 15R etc.) was controllable by lateral growth of the epitaxial layers parallel to (0001)-oriented surface. After chemical cleaning of the substrate surface, a 10 nm-thick sacrificial oxide (SiO_x) layer was grown on the SiC substrate by dry-oxidation at 1423 K for 60 min. The electrode patterns were made by removing the SiO_x layers, where contact metals were deposited by dipping in 5 % diluted hydrofluoric acid solution for 1 min using a photolithography technique. Prior to the deposition of contact materials, the substrates were cleaned by deionized water. Then, Ti and Al stacking layers with high purities were deposited sequentially on the substrate in a high vacuum chamber where the base pressure was below 5×10^{-6} Pa. The thicknesses of the Ti and Al layers investigated in this study are 100 nm and 380 nm, respectively, and these layer thicknesses were chosen to give the average composition of the Ti(20 at%) and Al(80 at%), where the layer thicknesses were measured by a quartz oscillator during deposition. The reasons to choose this average composition was that aluminum rich (more than 75 at%) in TiAl contacts were empirically found to be essential to yield low contact resistance, resulting from formation of the Ti₃SiC₂ compound layers. After depositing, the binary TiAl contact layers were annealed at 1273 K for a storage time of 2 min in an ultra-high vacuum chamber where the vacuum pressure was below 1×10^{-7} Pa.

The surface morphology of the TiAl contact layers on 4H-SiC after annealing was observed using a JEOL JSM-6060 scanning electron microscope (SEM). Microstructural analysis and identification of the Ti₃SiC₂ layers at the contact layers/4H-SiC interfaces after annealing was performed using X-ray diffraction (XRD) and cross-sectional TEM. For XRD analysis, Rigaku RINT-2500 with Cu $K\alpha$ radiation operated at 30 kV and 100 mA was used. In particular, the interfacial structures and an orientation relationship between the contact layers and the 4H-SiC substrates were characterized by cross-sectional high-resolution TEM observations and selected area diffraction pattern (SADP) analysis, respectively, using a JEOL JEM-4000EX electron microscope operated at an accelerating voltage of 400 kV, where the point-to-point resolution of this microscope was approximately 0.17 nm. Z-contrast images were obtained using a spherical aberration (C_s) corrected scanning transmission electron microscope (STEM) (JEOL 2100F), which provides an unprecedented opportunity to investigated atomic-scale structure with a sub-Å electron probe. Thin foil specimens for the TEM and STEM observations were prepared by the standard procedures: cutting, gluing, mechanical grinding, dimple polishing, and argon ion sputter thinning techniques.

Calculations of electronic structure and total energy were carried out using the Vienna *ab initio* simulation package (VASP) within the framework of density functional theory (DFT) [21]. The projector augmented wave method was used for electron-ion interactions, and the generalized gradient approximation of Perdew et al. (PW91) was employed to describe the

exchange-correlation functional. The single-particle Kohn-Sham wave function was expanded using plane waves with different cutoff energies depending on the calculated systems. Sampling of irreducible Brillion zone was performed with a regular Monkhorst-Pack grid of special k points, and electronic occupancies were determined according to the Methfessel-Paxton scheme. Independent k point convergence tests were conducted for distinct supercells. Ground state charge densities were calculated self-consistently using a Pulay-like mixing scheme and the stable blocked Davidson minimization algorithm. Total energies were calculated using the linear tetrahedron method with Blöchl corrections, which eliminates broadening-related uncertainties. All atoms were fully relaxed using the conjugate gradient algorithm until the magnitude of the Hellmann-Feynman force on each atom converged to less than 0.05 eV/\AA , yielding optimized structures.

To determine the most stable interface theoretically, one first has to establish feasible models on the basis of the distinct terminations and contact sites and then compare them. However, a direct comparison of total energies of such candidate models is not physically meaningful since interfaces might have a different number of atoms. On the other hand, the adhesion energy (W_{ad}), which is key to predicting the mechanical properties of an interface, is physically comparable. Generally, the W_{ad} is defined as the energy required to reversibly separate an interface into two free surfaces, neglecting plastic and diffusion degrees of freedom. The energy needed in actual cleavage experiments is always greater than the W_{ad} owing to plastic deformation, but the extent of plastic deformation relies on the W_{ad} . Formally, the W_{ad} can be expressed in terms of surface and interfacial energies or by the difference in total energy between the interface and isolated slabs [22,23]:

$$W_{\text{ad}} \equiv \sigma_1 + \sigma_2 - \sigma_{12} = (E_1 + E_2 - E_{\text{IF}}) / A \quad (1)$$

Here σ_i is the surface energy of slab i , σ_{12} is the interface energy, E_i is the total energy of isolated slab i , E_{IF} is the total energy of the interface system, and A is the total interface area. In general, two steps can be taken to estimate the W_{ad} . First, the total energies were calculated for a series of separations as two rigid slabs were brought increasingly closer from a large initial separation. As a consequence, the calculated total energies were found to behave like a parabola, passing through a minimum at the equilibrium separation. The unrelaxed W_{ad} was obtained by computing the energy difference between the interface at the equilibrium state and the unrelaxed isolated slab. Next, each isolated slab as well as interfacial slab was allowed to optimize fully, yielding an estimation of relaxed W_{ad} .

2.1. Atomic-scale structures of the Ohmic contacts

The electric properties for the TiAl contact systems before and after annealing are measured first to verify the formation of Ohmic contact. The current almost keeps zero before the annealing, while increasing nearly linear with the rise of applied bias, which unambiguously confirms the formation of the Ohmic contacts after annealing. Further XRD analyses demonstrate that a new reaction product, the ternary Ti_3SiC_2 , is generated after annealing, which shows a strongly (0001)-oriented texture. The SiC retains (0001)-oriented texture after annealing, there-

by facilitating development of hetero-epitaxy between reaction products and substrates. The TEM imaging reveals that no any other compounds contact directly the SiC surface, thereby ensuring an exclusive contact of Ti_3SiC_2 to SiC. Since the carbide itself is metallic in nature, the lowering in Schottky barrier in the TiAl-based contacts is hence attributed qualitatively to the epitaxial and atomically sharp SiC/ Ti_3SiC_2 interface. A careful indexing of the selected area diffraction pattern (SADP) at the contacts/SiC interface reveals that the formed Ti_3SiC_2 layers have epitaxial orientation relationships, that is, $(0001)\text{Ti}_3\text{SiC}_2// (0001)\text{SiC}$ and $[0\bar{1}10]\text{Ti}_3\text{SiC}_2// [0\bar{1}10]\text{SiC}$, with the SiC substrate. These orientation relationships are believed to be beneficial for forming a coherent and well matched interface between SiC and Ti_3SiC_2 , since they both belong to the hexagonal space group with lattice constants of $a = 3.081 \text{ \AA}$ and $c = 10.085 \text{ \AA}$ for the SiC and $a = 3.068 \text{ \AA}$ and $c = 17.669 \text{ \AA}$ for the Ti_3SiC_2 .

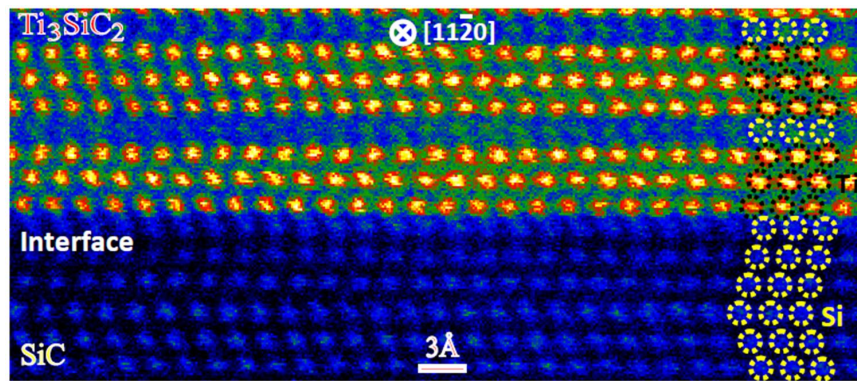


Figure 1. A typical HAADF-STEM image of the SiC/ Ti_3SiC_2 interface in the annealed TiAl contact system observed from $[11\bar{2}0]$ direction. The points at which the phase contrast is no longer periodic in either the Ti_3SiC_2 or SiC define the interfacial region [23].

A representative HAADF image of the SiC/ Ti_3SiC_2 interface is shown in Fig. 1, which confirms a clean and atomically sharp contact between the two materials. Since intensity of an atomic column in the Scanning TEM, to good approximation, is directly proportional to the square of atomic number (Z) [24], brighter spots in image represent atomic columns of Ti, while the comparatively darker ones are Si. Not surprisingly, the columns of C are not scattered strongly enough to be visualized owing to its small Z , thereby making this image incomplete. It should be noted that obtaining a signal of pure interfacial carbon is technically very difficult because the specimen can be easily affected by the environmental carbon, thereby precluding the element-selective imaging of carbon. We therefore rely on the first-principles calculations instead to discuss the possibility in the presence of C at the interface, as will be described later. To see the interface clearer, we magnify the cross-sectional HAADF image in Fig. 2(a) and further filter it to reduce noise, as shown in Fig. 2(b). The Si-terminated Ti_3SiC_2 is observed intuitively to make a direct contact with the Si-terminated SiC substrate with interfacial Si atoms of Ti_3SiC_2 sitting above hollow sites of interfacial Si plane of SiC. However, this straightforward interpretation is premature, as will be described later. Since there are no pits, spikes, or dislocations that might act as pathways for current

transport, we conclude that this clean and coherent SiC/Ti₃SiC₂ interface should be critical for the formation of Ohmic contact.

To clarify the mechanism, it is prerequisite to determine the atomic structure of the SiC/Ti₃SiC₂ interface via complementing the obtained HAADF image (Fig. 1). We have considered a total of 96 candidate interfacial geometries using bulklike slabs, taking into account termination effect, stacking sequence, and full optimization. From the bulk 4H-SiC and Ti₃SiC₂ structures and the relative stacking order of Ti and Si, the observed image in Fig. 2(a) can be intuitively fitted by a SiSi model shown in Fig. 2(c). In this model, the interfacial Si atoms of Ti₃SiC₂ sit above the hollow sites of interfacial Si plane of SiC, where the optimal distance between interfacial Si-Si planes (denoted as $d1$ in Fig. 2(b)) and that between interfacial Si-Si atoms projected onto paper plane (denoted as $d2$ in Fig. 2(c)) are calculated to be 2.13 and 2.53 Å, respectively. These distances, however, deviate severely from their average experimental values, 2.5 Å and 2.8 Å, which are obtained by characterizing quantitatively the HAADF image (Fig. 2(a)). In addition, an examination of interface stability by calculating the W_{ad} indicates that this SiSi model is not favored (1.62 J/m²). It is even less stable than the model with interfacial Si of Ti₃SiC₂ resting straight atop the interfacial Si of SiC (2.58 J/m²), which contravenes again the observed image.

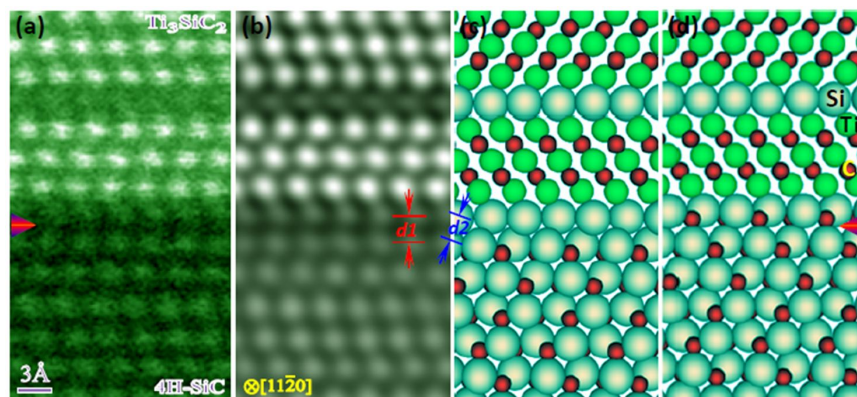


Figure 2. a) Magnified HAADF image of the SiC/Ti₃SiC₂ interface. (b) The same image as in (a) but has been low-pass filtered to reduce noise. Relaxed SiC(0001)/Ti₃SiC₂(0001) interface models (c) without (SiSi) and (d) with (SiCSi) interfacial C atoms. The distance between interfacial Si-Si layers is represented by $d1$ and that between interfacial Si-Si atoms projected onto the paper plane by $d2$. The interfaces are represented by an arrow [23].

To resolve these paradoxes, we notice that a possibility might be ignored, that is, the unseen C might be trapped at the interface, altering local environment there. To test this scenario, we established a new model (named SiCSi) by introducing C into the interfacial layer from the consideration of crystal extension and stacking sequences. The calculated W_{ad} of this SiCSi model is 6.81 J/m², which indicates that interface is indeed strengthened substantially after incorporating C. Further examination of the relaxed atomic geometry (Fig. 2(d)) reveals that the incorporation of C does not induce a significant structural transformation. Namely, the two Si layers proximal to the interface maintain the stacking seen in Fig. 2(c), thus matching the HAADF image geometrically. Quantitatively, the $d1$ and $d2$ distances are now 2.53 and 2.81 Å, respective-

ly, very close to the experimental values. Therefore, the introduction of interfacial C monolayer resolves the inconsistencies between simulations and experiments.

2.2. Electronic structure and bonding

Calculations of *p*-type Schottky barrier height (SBH) reveal that the interface with C (0.60 eV) has much lower SBH than the interface without C (1.05 eV), suggesting that the trapped C assist the lowering of SBH. To shed light on origin of the decrease in SBH and junction strengthening in the SiCSi interface, we characterized thoroughly interfacial electronic states and bonding nature. Figure 3(a) shows a planar-averaged charge-density difference along interface normal, where there appears a more dramatic accumulation of charge within the interfacial region for the interface with C. This indicates that the covalent bonding is strengthened in the SiCSi case. In addition, we note that the planar-averaged density difference for the SiCSi more prominently deviates from zero around interface, reflecting more significant charge transfer between the SiC and Ti_3SiC_2 slabs. Moreover, charge is observed to be depleted noticeably in both the sub-interfacial SiC and Ti_3SiC_2 region for the SiCSi, suggesting that the atoms second nearest to the interface contribute to interfacial bonding. These missing charges, to a large extent, make their way onto the more electronegative C ions, indicative of the formation of ionic bonding.

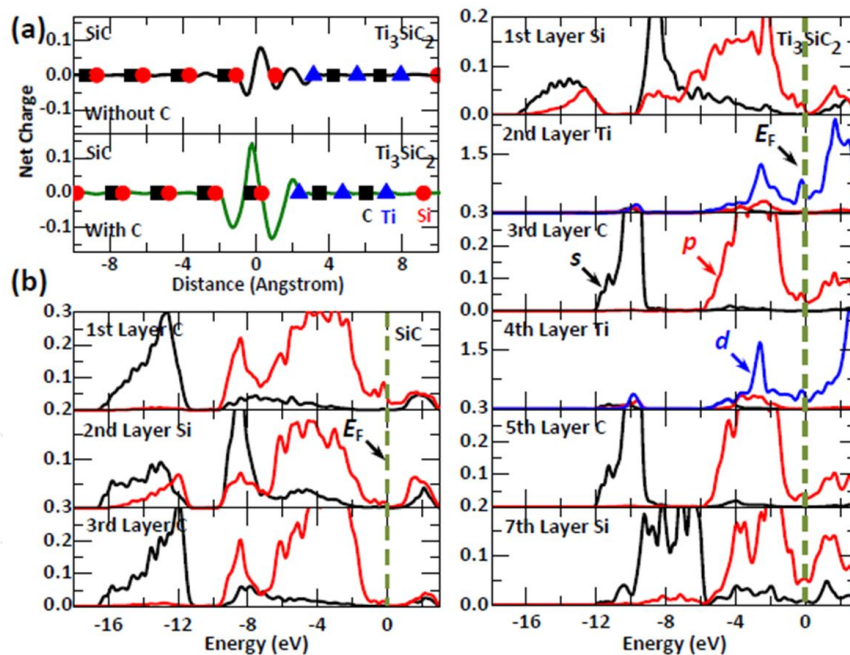


Figure 3. a) Planar-averaged charge-density difference for the relaxed interfaces with and without C along [0001] direction. (b) Density of states projected onto the atomic layers close to the relaxed SiCSi interface. The left bottom panel shows the PDOSs of SiC layers and the right one those of Ti_3SiC_2 layers. The first layer is the atomic layer proximal to interface. The E_F is set to zero [23].

We then presented in Fig. 3(b) DOS projected on selected atomic layers of the SiCSi interface. A key feature in this figure is that a strong interaction is observed between the sub-

interfacial Ti d and Si p states below Fermi level (E_F), which continues well into SiC surface, inducing noticeable gap states in the interfacial C at E_F . This means that the interfacial C layer is metalized, indicative of possible electric conductivity. In fact, the gap states can extend as far as they can into deeper layers of SiC, as there appear weak but visible peaks at E_F in the PDOSs of the 2nd and 3rd layers of SiC. Therefore, a local weak metallicity might occur at top few layers of the semiconductor surface, which could enable current flow through the SiC. We also note significant hybridization between the interfacial C sp and Si sp states, suggestive of covalent bonding at interface.

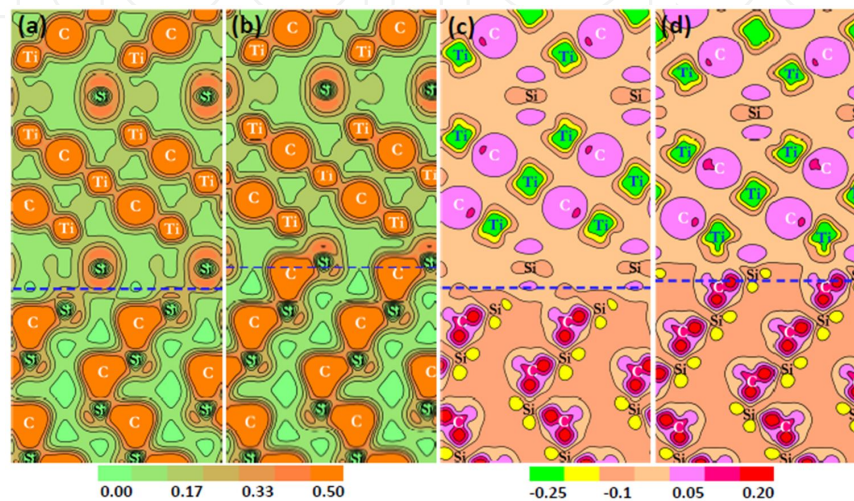


Figure 4. Contour plots of charge densities for (a) SiSi and (b) SiCSi interfaces taken along (11-20) plane. The interface is represented by a horizontal line and the atoms that intersect the contour plane are labeled. Corresponding contour plots of charge-density differences for (c) SiSi and (d) SiCSi interfaces [23].

Figure 4 shows contour plots of charge densities and their differences along (11-20) plane for the optimized SiSi and SiCSi interfaces. We notice in Fig. 4(b) that the bonding interaction between interfacial Si and C for the SiCSi interface is remarkably similar to the Si-C interaction deeper into SiC: the majority of charge is localized on C with humps directed towards their neighboring Si. We thus conclude that the interfacial bonding for the SiCSi is of mixed covalent-ionic nature. The interfacial bonds for the SiSi interface, however, have covalent nature with a small amount of charge accumulated within the interfacial region (Fig. 4(a)). In addition, the amount of charge accumulated on the interfacial Si-Si bonds of SiSi (Fig. 4(c)) is far less significant than that on the interfacial Si-C bonds of SiCSi (Fig. 4(d)). This heavier charge accumulation in the case of SiCSi, together with its mixed covalent-ionic character at interface, accounts for the largest W_{ad} associated with the SiCSi interface.

2.3. Quantum electron transport properties

Although the charge-distribution analysis can reveal valuable information on interfacial bonding, it provides restrained insight into how electrons distribute around E_F , which matters because density around E_F directly determines the current transmission. Figure 5 illustrates an electron-density isosurface and its slice along the (11-20) plane for the optimized

SiCSi interface around E_F . From Fig. 5(a), one can see that charges surrounding interfacial Si are connected and broadly distributed in a sheet-like fashion, which suggests possible electrical conductivity through this region. In addition, there also appear heavily accumulated electrons within the interfacial area, which are connected along the interface and extended as far as several atomic layers into the SiC. These characters can also be confirmed from the slice plot in Fig. 5(b), meaning that current might flow over top few atomic layers of semiconductor, thereby causing Ohmic property. As expected, the electron density at E_F is extremely high for the Ti_3SiC_2 (*i.e.*, sea of electrons) but becomes nil for the SiC layers away from interface (Fig. 5(b)), which can be understood from their intrinsic metallic and semi-conducting nature [25].

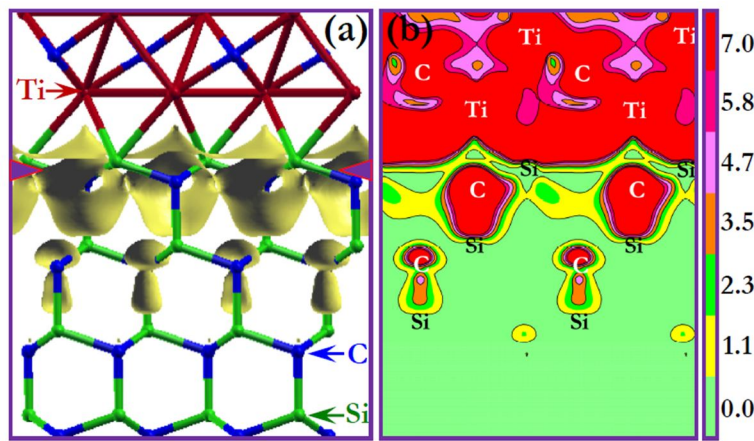


Figure 5. a) Isosurface and (b) electron density plot along the (11-20) plane in the energy window ($E_F - 0.5 \text{ eV}$, E_F) for the SiCSi interface. The interface is marked by two arrows [18].

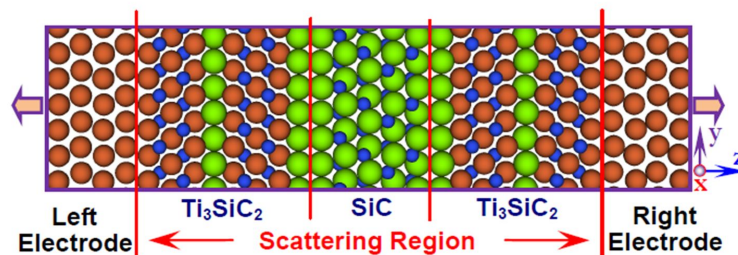


Figure 6. Schematic illustration of a two-probe $\text{Ti}/\text{Ti}_3\text{SiC}_2/\text{SiC}/\text{Ti}_3\text{SiC}_2/\text{Ti}$ quantum transport system. The system has infinite extent in the (x, y) direction and extends to $\pm\infty$ in the z direction. The $\text{SiC}/\text{Ti}_3\text{SiC}_2$ interfaces shown in Fig. 2 are adopted [18].

To examine electrical conductivity and gain insight into how the interface influences current transport, we devised a two-probe system [26], $\text{Ti}/\text{Ti}_3\text{SiC}_2/\text{SiC}/\text{Ti}_3\text{SiC}_2/\text{Ti}$, and investigated nonequilibrium quantum transport properties. Figure 6 schematically shows a model of the sandwich transport system, which can be divided into a left semi-infinite electrode, a scattering region, and a right semi-infinite electrode. The atomic and electronic structures of the

semi-infinite Ti electrodes are assumed to be the same as those of bulk Ti. On the other hand, the electronic states of scattering region are calculated self-consistently. The scattering region consists of hexagonal SiC and Ti_3SiC_2 layers and the periodic boundary conditions are imposed along the directions parallel to the interface. The SiC/ Ti_3SiC_2 interface could be either the SiSi or SiCSi, whereas other interfaces are maintained identical for the sandwich systems. In this sense, the difference between the two systems can be mainly attributed to their differing SiC/ Ti_3SiC_2 interfaces. Furthermore, we also calculated the Ti/SiC/Ti system, wherein the SiTi model was taken as the SiC/Ti interface.

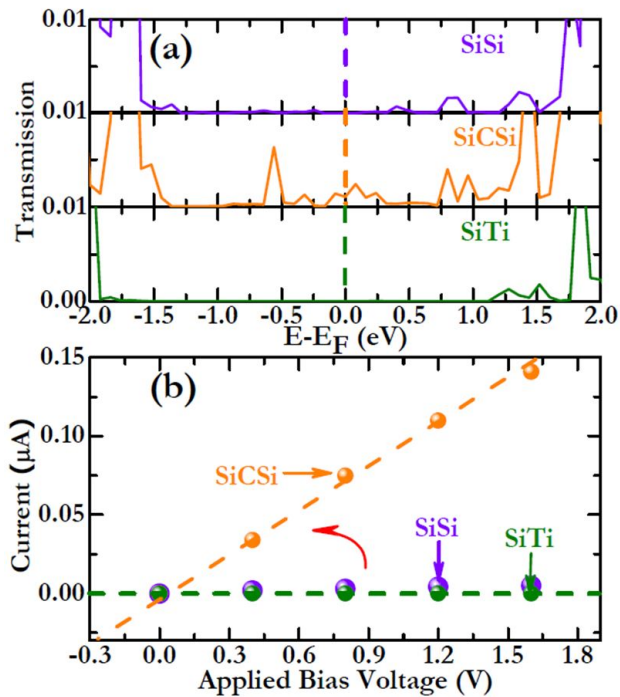


Figure 7. a) Transmission spectra under 0 V and (b) current-voltage characteristics for the sandwich systems involving the interfaces containing direct Si-Si bonding (SiSi), Si-C-Si bonding (SiCSi), and the direct contact of Ti to SiC (SiTi). Refer to Fig. 2 for their corresponding interfacial configurations [18].

Figure 7(a) shows transmission spectra for the relaxed SiSi, SiCSi, and SiTi systems, where one can see that the spectra differ from one another suggesting variations in electronic structures with interface geometries. The most interesting feature is the presence of transmission peaks at E_F for the SiCSi, which is attributable to the electrons distributed around the interface at E_F . Further calculations on electrical properties (*e.g.*, I - V curve) for the three systems reveal that the current in the SiCSi case increases much faster than either the SiSi or SiTi case as the applied bias voltage increases (Fig. 7(b)), which can be explained by its lowest SBH. We further examined how applied bias voltages vary from the interface to the SiC region by analyzing the difference in effective potential along the (11-20) plane between the bias voltage of 0.4 V and the one of 0.0 V for the relaxed system. The voltage is found to drop less intensively from the interface to the SiC in the SiC-Si case, suggestive of less Schottky nature. Finally, in comparing the general trend of the calculated I - V with that of our experimental curve, we find that they agree qualitatively:

both the annealed specimen and the SiCSi model clearly show Ohmic behavior, thereby validating the application of the SiCSi model to describe the Ohmic contacts in the TiAl-based system. In addition to the role of this interface, we also found that an atomic-scale Ti_3SiC_2 -like bilayer can be embedded in the SiC interior, forming an atomically ordered multilayer that exhibits an unexpected electronic state with point Fermi surface. The valence charge is confined largely to this bilayer in a spatially connected fashion, serving possibly as a conducting channel to enhance the current flow over the semiconductor.

3. Atomic-scale Ti_3SiC_2 bilayers embedded in SiC

3.1. Atomic structure of the embedded system

Figure 8(a) shows a HAADF image of the annealed TiAl/SiC system, where the SiC substrate is covered entirely by a layered compound, Ti_3SiC_2 , as reported previously. In addition to the formation of this epitaxial and coherent SiC/ Ti_3SiC_2 interface, another interesting feature is that an atomic-scale bilayer is generated in the SiC interior (marked by a square in Fig. 8(a)), which is located approximately 9.5 nm away from the interface. An enlarged image of the region surrounding the bilayer shows that it has a Ti_3SiC_2 -like structure, as shown in Fig. 8(b), where brighter spots represent atomic columns of Ti (smaller circles), while dark ones those of Si (larger circles), since intensity of an atomic column in STEM is, to a good approximation, directly proportional to $Z^{1.7}$ (Z : atomic number) [24].

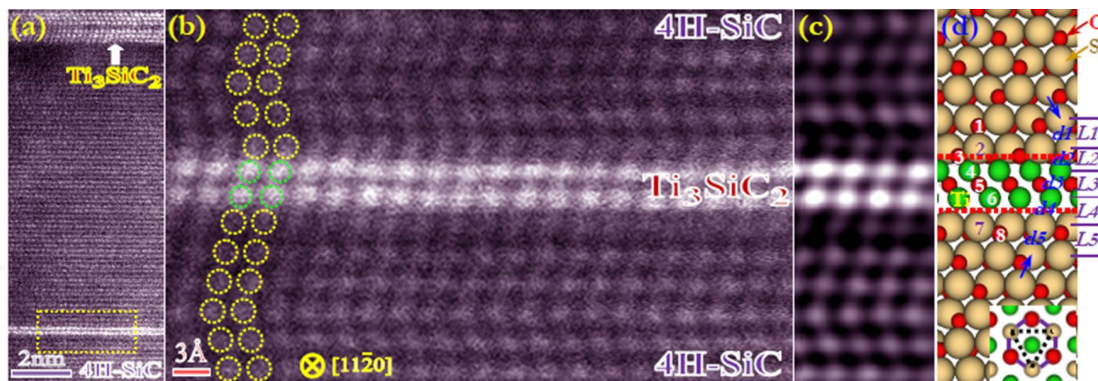


Figure 8. a) HAADF-STEM image for the Ti_3SiC_2 -like bilayer embedded in 4H-SiC in the annealed TiAl contact system viewed along $[11\bar{2}0]$ direction. The bilayer sits about 9.5 nm below the SiC/ Ti_3SiC_2 interface. (b) Magnified HAADF image of the region marked in (a) by a dotted square. An overlay is given, where the big circles indicate Si and small ones Ti. (c) The same image as in (b) but has been low-pass filtered to reduce noise. (d) The optimized SiC/ Ti_3SiC_2 /SiC multilayer model. The distances between layers around the bilayer are represented by L_m ($m = 1$ to 5) and those between neighboring atoms projected onto the paper plane by d_m . The atomic layers are labeled 1 through 8. The inset shows top view of arrangement of Ti and its neighboring Si and C, where the Ti occupies atop the center of the hexagon composed of Si and C [19].

Evidently, the bilayer is embedded in the SiC in an atomically coherent and ordered fashion with no transitional or intermixing layers (see Fig. 8(c)). In view of bulk structures of 4H-SiC and Ti_3SiC_2 and the relative stacking sequence of Ti and Si, the image in Fig. 8(c) can be

qualitatively fitted by an energetically stable model shown in Fig. 8(d). In this model, the optimal distances between layers around the bilayer (denoted as $L1$ to $L5$ in Fig. 8(d)) are calculated to be 2.52, 2.27, 2.28, 2.40, and 2.57 Å, respectively, very close to experimental values of 2.5, 2.2, 2.3, 2.3, and 2.7 Å estimated via quantitative characterization and averaging of different sites in the HAADF images. In addition, the calculated distances between neighboring atoms (labeled $d1$ to $d5$ in Fig. 8(d)) (2.67, 2.44, 2.44, 2.55, and 2.72 Å) also approach the experimental values (2.7, 2.3, 2.4, 2.6, and 2.7 Å). These mean that the model constructed (Fig. 8(d)) matches the HAADF image (Fig. 8(c)) both qualitatively and quantitatively in light of energetics and atomic distances.

3.2. Formation of point Fermi surface

To gain insight into how the embedded layer influences SiC electronically, we present in Fig. 9 band structure and density of states (DOS) of the multilayer system calculated using the optimal atomic geometry (Fig. 8(d)). Unexpectedly, several bands with a quadratic dispersion cross the Fermi level (E_F) at a single Γ point (Fig. 9(a)), rendering conduction bands (CB) and valence band (VB) touch at their tips and hence the multilayer become a gapless semiconductor. Inspection throughout the Brillion zone verifies that the Fermi surface crossing is a single point, which determines E_F , as in the bilayer graphene with no external stimuli (bands in graphene extend linearly both to lower and higher energy from point Fermi surfaces, as referred to as “massless Dirac”). This crossing of bands is confirmed in the DOS showing a curious vanishing of states at E_F for both spins (Fig. 9(b)) and further verified in a surface plot of the two bands proximal to E_F in a small k space presenting gapless character at the Γ point and a gap in the region away from the crossing point (Fig. 2(c)).

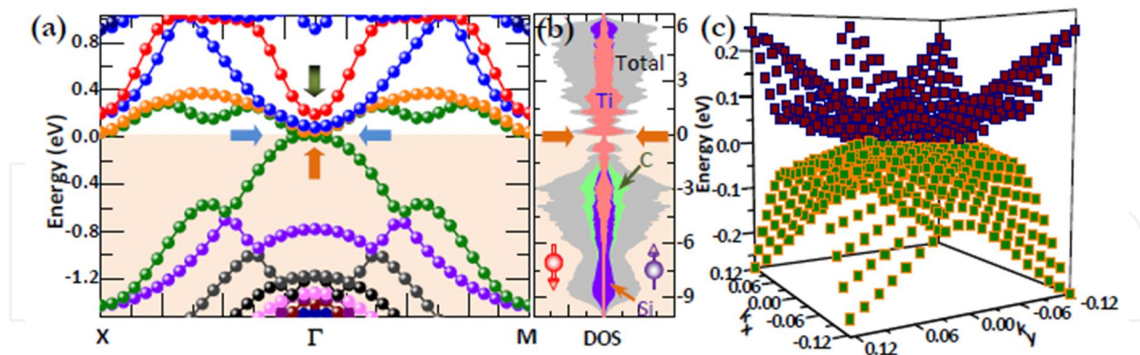


Figure 9. a) Blowup of band structure around E_F shown on the xy plane with $X = \pi/a(1, \hat{1}, 0)$ and $M = \pi/a(1, 1, 0)$, where the “ a ” is in-plane lattice constant. Note that the point Fermi surface is at Γ where bands cross precisely at E_F . (b) Total DOS and PDOS plots of C, Si, and Ti atom contributions for the optimized SiC/Ti₃SiC₂/SiC multilayer, showing that bands surrounding E_F have characters of Ti in the bilayer. (c) “Surface” plot of the two bands that cross the E_F , centered surrounding the Γ point. The E_F position is aligned to zero [19].

In addition, extensive calculations using the LDA and PBE functional corroborate once again the peculiar crossing of the bands (band structure and DOS spectra are almost identical to those calculated using the PW91), which therefore indicates that the crossing at E_F is not an

accidental degeneracy arising from the applied functional. This behavior is quite unusual, as it turns up neither in the SiC bulk showing E_F lying in a gap between states nor in the Ti_3SiC_2 bulk showing E_F lying in the middle of a band of electronic states, which can be attributed to the structural symmetry with Ti atoms sitting exactly atop center of the hexagon composed of Si and C (corresponding to the Γ point in k space), as shown in inset of Fig. 8(d). Further calculations reveal that this gapless nature appears in the multilayer consisting of a Ti_3SiC_2 -like monolayer embedded in SiC as well, indicating that the unique state could be understood upon quantum confinement effect and the interface phenomenon accompanied by the polarity discontinuity. However, our additional calculations suggest that the point Fermi surface vanishes when a Ti_3SiC_2 trilayer is hypothetically embedded within SiC, which takes on metallic states with three bands (arise from the three Ti layers) crossing E_F , similar to what is seen in the band structure of Ti_3SiC_2 bulk. This transition from the zero-gap semiconductor to metal therefore highlight the importance of quantum confinement in inducing the point Fermi surface, since additional layer is believed to relieve the confinement effect and produce more states.

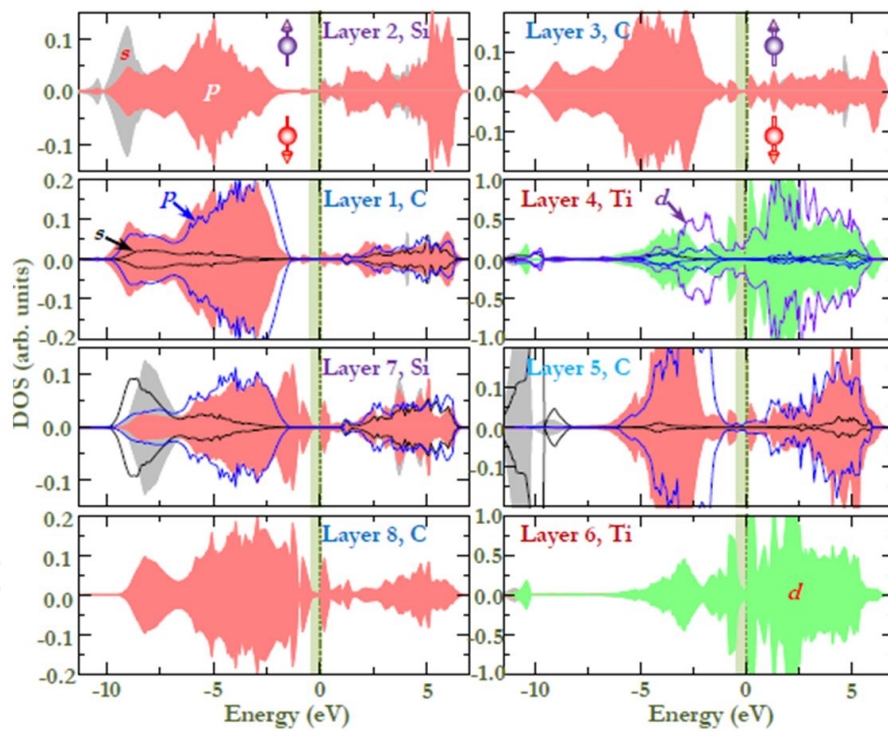


Figure 10. DOS projected on selected atomic layers in the multilayer system. Left panel gives the PDOSs of SiC layers and right panel those of Ti_3SiC_2 layers. The lines show PDOSs of the corresponding atoms in the bulk as a reference. The E_F is set to zero [19].

3.3. Electronic states

Further investigation of DOS projected on selected atomic layers provides evidence that the bands close to E_F involve dominantly Ti 3d states (layers 4 and 6 in Fig. 8(d)). These states

undergo a sudden vanishing at E_F (Fig. 10), which is in stark difference from what is seen in the DOS projected (PDOS) on Ti in bulk Ti_3SiC_2 presenting continuous states at and around E_F (lines in Fig. 10). In addition, there are notable electronic states in the forbidden gap of bulk SiC for the C and Si in the multilayer, which is definitely attributable to the embedded bilayer. The presence of the induced gap states, in particular, those below the CB minimum of bulk SiC but close to E_F , can readily present a trap for CB electrons, which could modify electronic behaviors of the originally insulating SiC and thus be relevant for the current flow over semiconductor in the TiAl-deposited SiC system. Moreover, we note that overall features of PDOS for identical atom species may even differ from one another, which can be ascribed to their different bonding environments.

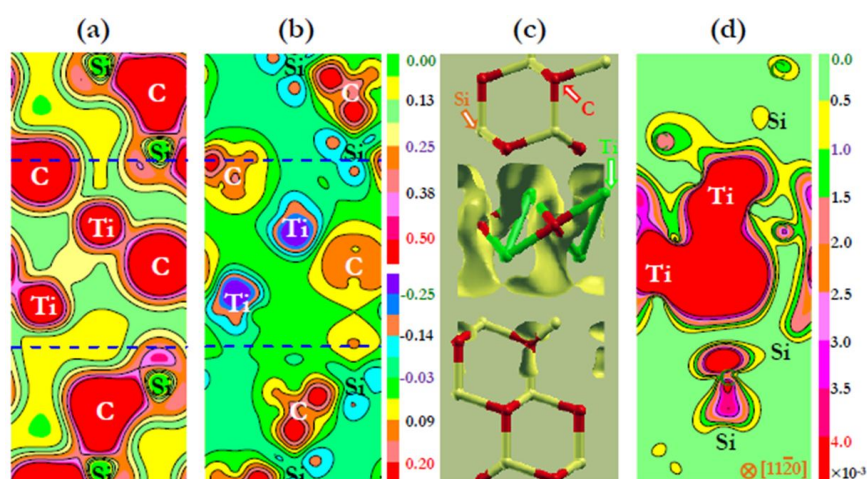


Figure 11. Contour plot of (a) charge density and (b) density difference for the multilayer system viewed along the (11-20) plane. The difference of charge density gives the redistribution of charge in the system relative to its isolated one. The upper scale denotes the magnitude of charge in (a) and the lower scale that of charge difference in (b). (c) Isosurface and (d) electron density plot along the same plane as in (a) in the energy window ($E_F - 0.5$ eV, E_F) [19].

To shed further light on bonding nature and charge distribution in the multilayer, we present contour plots of charge density (Fig. 11(a)) and its difference (Fig. 11(b)) along the (11-20) plane. From the figures, we notice that (i) majority of charge is localized on C atoms with humps distorted toward their neighboring atoms, suggesting that bonds in both SiC and bilayer are of a mixed covalent-ionic nature, (ii) charge distribution on C in SiC exhibits more pronounced lobes than that on C in the bilayer (Fig. 11(a)), indicative of more covalent element for bonds in SiC, and (iii) ionicity originates from the large charge gain on C at an expense of charge loss on its neighboring cations (Fig. 11(b)). Further examination on electron distribution around E_F reveals that valence electrons are confined, to a large extent, to within the bilayer (Fig. 11(c)), in good agreement with the DOS analysis (Fig. 3). These charges are spatially connected and broadly distributed surrounding the bilayer with a small degree of leakage into as far as two atomic layers of SiC (Fig. 11(c)), as is further confirmed from a slice plot in Fig. 11(d). This implies that the bilayer buried in between the SiC may act as a conducting channel so as to enhance current flow over the semiconductor.

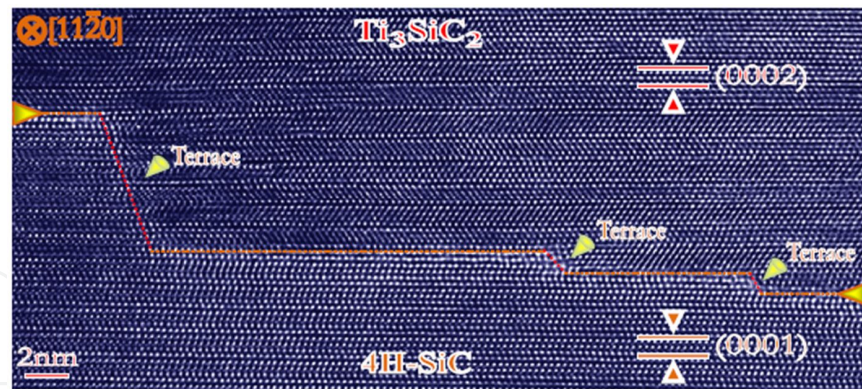


Figure 12. A cross-sectional HRTEM image of the contact of the formed Ti_3SiC_2 to the 4H-SiC substrate viewed from the [11-20] direction. The two materials are demarcated by a zigzag line. Terraces with varying dimensions are observed, as indicated by arrows [20].

4. Terraces at Ohmic contact in SiC electronics

Combining imaging with atomistic simulations, we determine the atomic-scale structures of terraces in between SiC and its contacts and relate the structures to their electronic states and bonding nature, aimed at revealing the impact of the terraces on the contacts of SiC electronics. The terraces were first characterized using the high-resolution TEM (HRTEM) and scanning TEM (STEM), upon which the first-principles calculations were performed. The combined study allows a deeper understanding of the role played by terraces in the ohmic contact formation on a quantum level. The terraces are structurally epitaxial, coherent and atomically ordered, and theoretically predicted to have electronic states at Fermi level (E_F) regardless of their dimension.

4.1. Atomic structures of terraces

Figure 12 shows a typical cross-sectional HRTEM image of the contact of Ti_3SiC_2 to SiC which includes terraces of various dimensions. Well arranged (000 l)-oriented lattice fringes can be observed in both the SiC and Ti_3SiC_2 layers. The points at which the phase contrast is no longer periodic define the interfacial area, as indicated by a zigzag line. Evidently, the SiC substrate is covered entirely by the Ti_3SiC_2 layers even in the terrace region (arrows), meaning a direct contact of Ti_3SiC_2 to SiC at the terraces at atomic scale. The terraces are atomically abrupt and ordered, showing no amorphous layers, secondary-phase layers, contaminants, or transition areas. A small number of misfit dislocations are identified at the contact region (not shown here) due to the small lattice mismatch of SiC to Ti_3SiC_2 (less than 0.5%). Further analyses of selected area diffraction patterns reveal that the Ti_3SiC_2 layers have epitaxial orientation relationships, $(0001)\text{Ti}_3\text{SiC}_2 // (0001)\text{SiC}$ and $[0-110]\text{Ti}_3\text{SiC}_2 // [0-110]\text{SiC}$, with the SiC substrate.

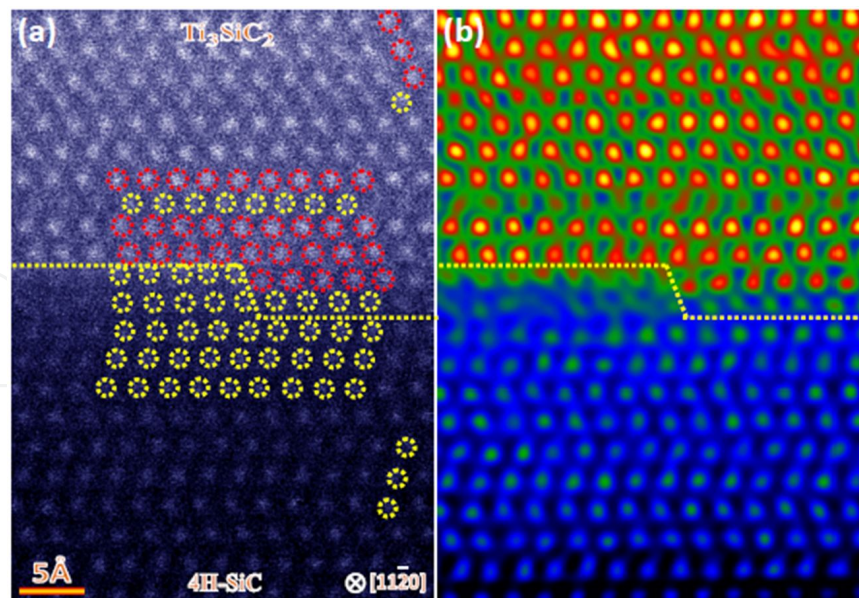


Figure 13. a) A typical HAADF-STEM image of a small terrace observed from the [11-20] direction. The terrace is indicated by a zigzag line. Bigger dotted circles denote Ti and the smaller ones Si. (b) The same image as in (a) but has been filtered to reduce noise [20].

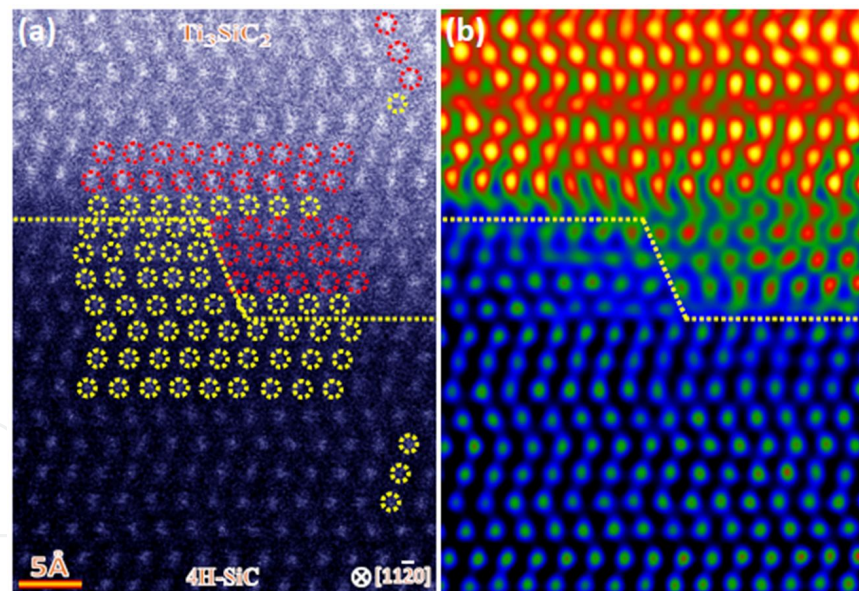


Figure 14. A typical HAADF image of an intermediate terrace observed from the [11-20] direction. The terrace is indicated by a zigzag line. (b) The same image as in (a) but has been filtered to reduce noise [20].

In general, this contact region contains terraces with a wide variety of dimensions that can be affected by numerous factors. However, to develop an understanding of such a complex contact, it is important to first focus on representative terraces. Here, we choose purposely three species of terraces based on the dimension: small, intermediate, and large terrace. The corresponding HAADF images are presented in Figs. 13–15, which confirm the atomically

abrupt and ordered terraces. Moreover, heteroepitaxy is retained between the SiC and Ti_3SiC_2 for each terrace. Since the intensity of an atomic column in the HAADF image is proportional to $Z^{1.7}$ (Z : atomic number) [24], brighter spots in the images represent atomic columns of Ti while darker ones are Si. In view of the atomic arrangements in the SiC and Ti_3SiC_2 bulks, we define the terrace by a dashed line and identify the atoms in a few layers close to the line as in the terrace region hereafter. For the small terrace, the image can be intuitively interpreted as a bonding of Ti (Si) in Ti_3SiC_2 to Si in SiC (Fig. 13(b)). However, this is not the case for the intermediate terrace showing Si-Si bonding at the hollow site (Fig. 14(b)). Further interpretation of the HAADF image of large terrace (Fig. 15(b)) reveals a Si-Si bonding as well. Not surprisingly, atomic columns of carbon are not scattered strongly enough to be visualized due to its small Z , rendering the image incomplete. Further complementing of these images so as to relate their atomic structures to their electronic properties requires a combination of imaging with the first-principles modeling.

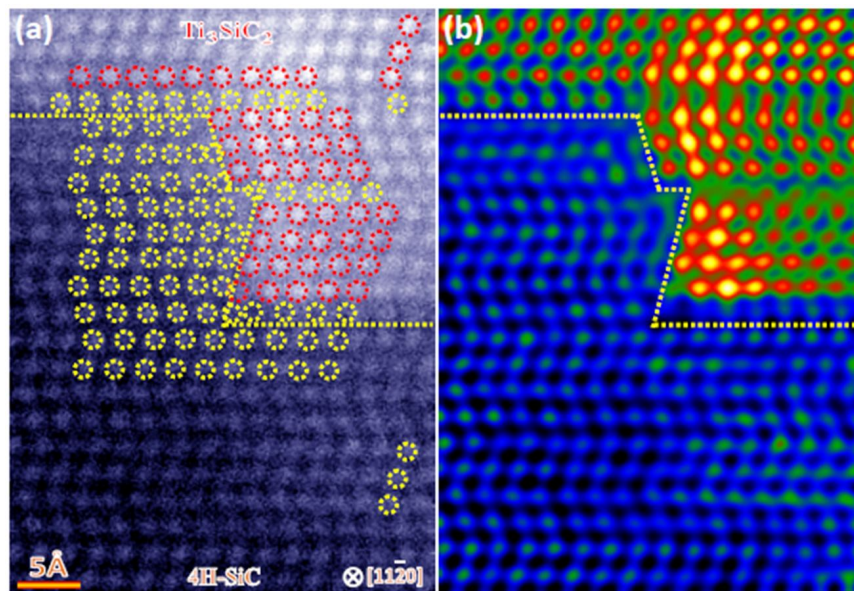


Figure 15. A typical HAADF image of a large terrace observed from the $[11\bar{2}0]$ direction. The terrace is indicated by a zigzag line. (b) The same image as in (a) but has been filtered to reduce noise [20].

4.2. Electronic states and bonding nature of the terraces

To gain insight into electronic properties of the terraces and the role they played in the ohmic contact formation, we perform first-principles calculations on the three typical terraces. Upon a consideration of bulk structures of SiC and Ti_3SiC_2 , the aforementioned orientation relations, and relative stacking sequence near terraces shown in the HAADF (Figs. 13–15), atomic models of the three representative terraces were established (Fig. 16), taking into account full structural relaxation. It should be noted that these models may not exactly reflect the real terraces because it is the extreme difficult to interpret directly the HAADF images owing to the intricate atomic arrangements around the terraces and to the invisible C atoms.

However, these models are constructed upon a careful consideration of the space filling and local chemical environment, and importantly they exhibit the typical variations of the contact with terraces, which should be useful as an initial stage to look at the electronic states of terraces. It is also worthy of mentioning that neither the total nor the interface energies could be applicable to justify the models as an interpretation of the HAADF images because (i) the terrace models have a different number of atoms, (ii) it is unlikely to calculate the exact total terrace area, and (iii) there are numerous candidates for each type of terrace. In the optimized model of small terrace (Fig. 16(a)), one can notice a bonding of Ti (Si) atoms in Ti_3SiC_2 to Si atoms in SiC at the hollow site.

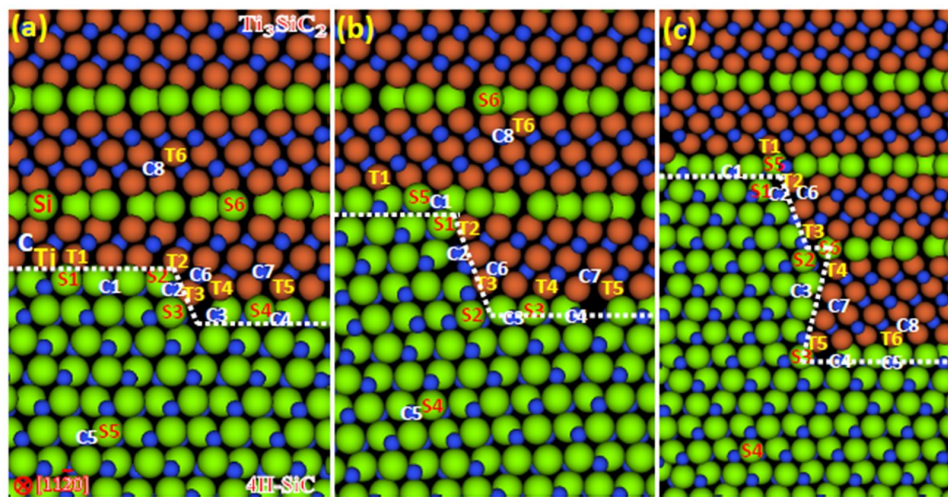


Figure 16. The relaxed atomic models of the three representative terraces with different dimensions: (a) small, (b) intermediate, and (c) large terrace. The representative atoms surrounding terrace are labeled for the atom-projected density of states analysis [20].

Figure 17 shows PDOS of several representative atoms at the small terrace (labeled in Fig. 17(a)), where a remarkable difference is seen between the atoms near and away from terrace. A key feature of this figure is that strong hybridization takes place between the Ti *d* (T1~T6) and Si *p* (S1~S6) levels below E_F , which continues well into the SiC region, inducing a pronounced gap state at E_F for the C atoms near the terrace (C1~C4, C6). However, such a gap state at E_F is vanished completely for the C deeper into the SiC (C5 in Fig. 17). Apart from the C, the Si atoms in SiC near terrace (S1~S3) also exhibit a weak yet visible peak at E_F that are totally absent in the bulk (S5 in Fig. 17). The presence of gap states can be attributed to the overlap of the Ti *d* with Si *p* levels. A notable hybridization is seen as well between the Si *sp* (S1~S4) and C *sp* (C1~C4, C6) levels, indicating the formation of covalency near terrace. Apart from the SiC, all of the atoms in Ti_3SiC_2 around terrace (C6, C7, S4, T1~T5) also exhibit a notable peak at E_F owing to the great degree of overlap between the Ti *d* and C (Si) *p* levels. Moreover, overall feature of PDOS for the Ti atoms around terrace (T1~T4) differs from that in the Ti_3SiC_2 bulk (T6), indicating that the terrace can have an impact on electronic states of Ti as well.

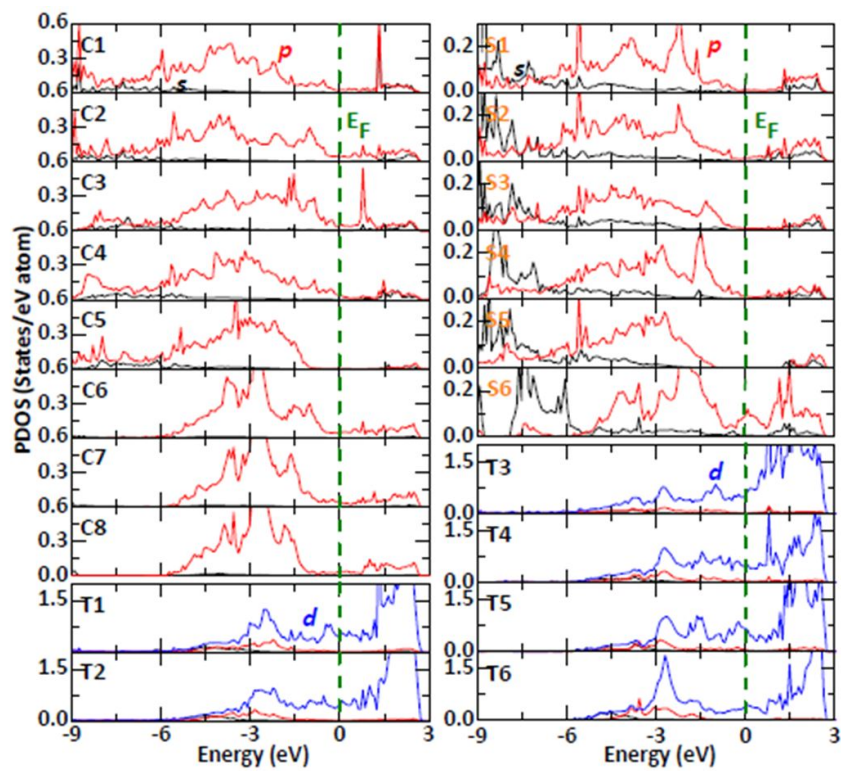


Figure 17. PDOS (states/eV atom) of several selected atoms near or far from the small terrace. All of atoms in the slab are fully relaxed. Refer to Fig. 16(a) for the sites of the selected atoms. The E_F is set to zero and indicated by a vertical dashed line [20].

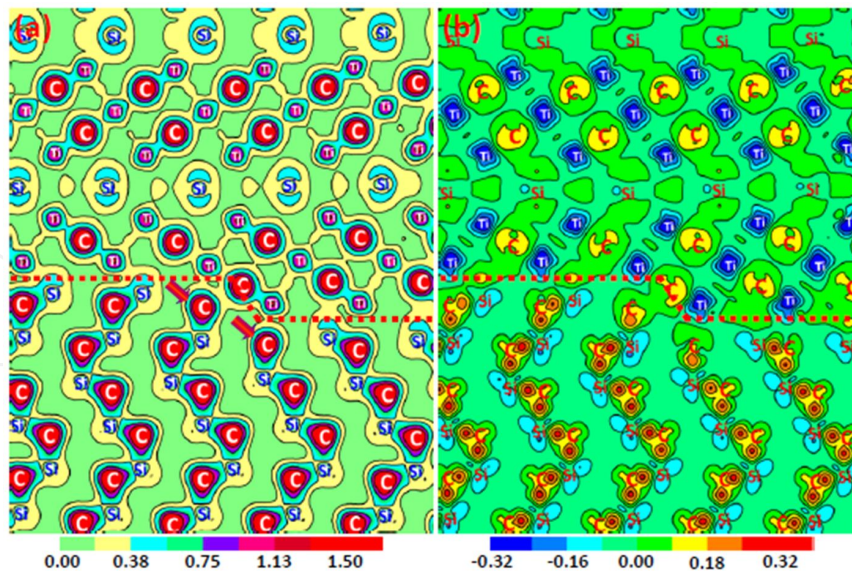


Figure 18. Contour plots of (a) charge density and (b) charge-density difference for the small terrace viewed along the (11-20) plane. Difference in charge density shows redistribution of charge near terrace relative to its isolated system. The position of terrace is indicated by a zigzag dashed line and the atoms intersecting the contour plane are labeled [20].

To identify the bonding nature directly, we further show the contour plots of charge density and density difference for the optimized small terrace viewed along the (11-20) plane (Fig. 18). From Fig. 18(a), a remarkable difference is observed in charge distribution on C: charge distribution around C in SiC (away from terrace) has humps directed toward neighboring Si, while that around C in Ti_3SiC_2 (away from terrace) is of almost spherical symmetry. However, the charge distribution on some C atoms near the terrace (indicated by arrows in Fig. 18(a)) shows a mixed character with a lobe on one side while a spherical outline on the other, which is reflected from their different PDOS (Fig. 17). Furthermore, the charge distribution on the Si-C bonds closet to the zigzag line (Fig. 18(a)) shares some features with that on the Si-C bonds away from the zigzag line (analog to the bonds in SiC bulk): (i) the majority of charges are distributed on all the C atoms, and (ii) there are visible distortions in the charge distribution on the C atoms directed toward their adjacent Si atoms. A certain level of covalency is seen on the atomic bonding along the zigzag line (which defines the terrace), which is due to the hybridization of Ti d with Si (C) p levels (Fig. 17). These imply a mixed covalent-ionic bonding for the small terrace. It is obvious from the density-difference plot (Fig. 18(b)) that the ionic nature arises from the charge transfer of Ti (Si) to C. In the Ti_3SiC_2 region away from the zigzag line, the Ti-C bonds are found to have more covalent element than the Ti-Si bonds, as more amount of charges are accumulated in between Ti and C, which indicates that the Ti-C is a stronger chemical bond than the Ti-Si.

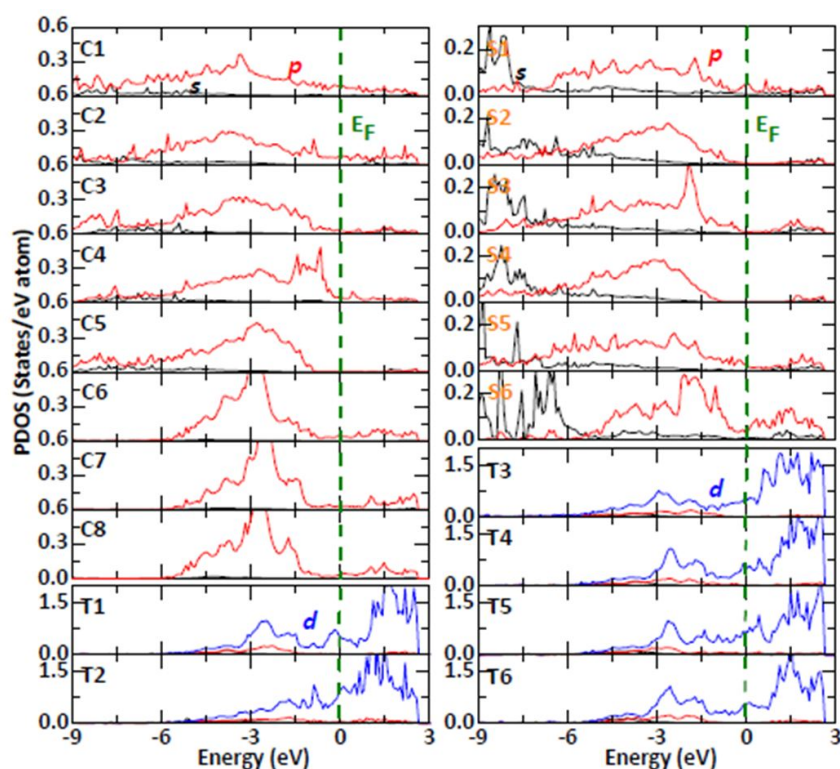


Figure 19. PDOS (states/eV atom) of several selected atoms at or far from the intermediate terrace. Refer to Fig. 16(b) for the sites of the selected atoms [20].

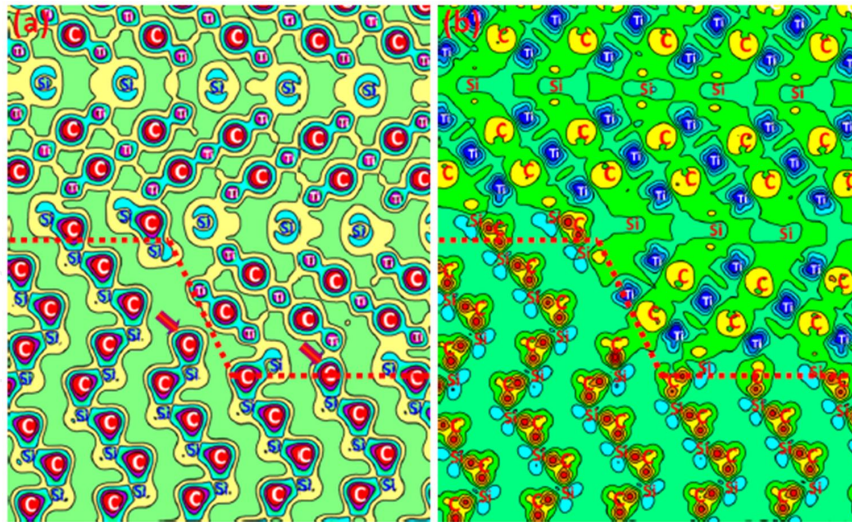


Figure 20. Contour plots of (a) charge density and (b) charge-density difference for the intermediate terrace viewed along the (11-20) plane. The scale is the same as in Fig. 18. The location of terrace is indicated by a zigzag line and the atoms intersecting the contour plane are labeled [20].

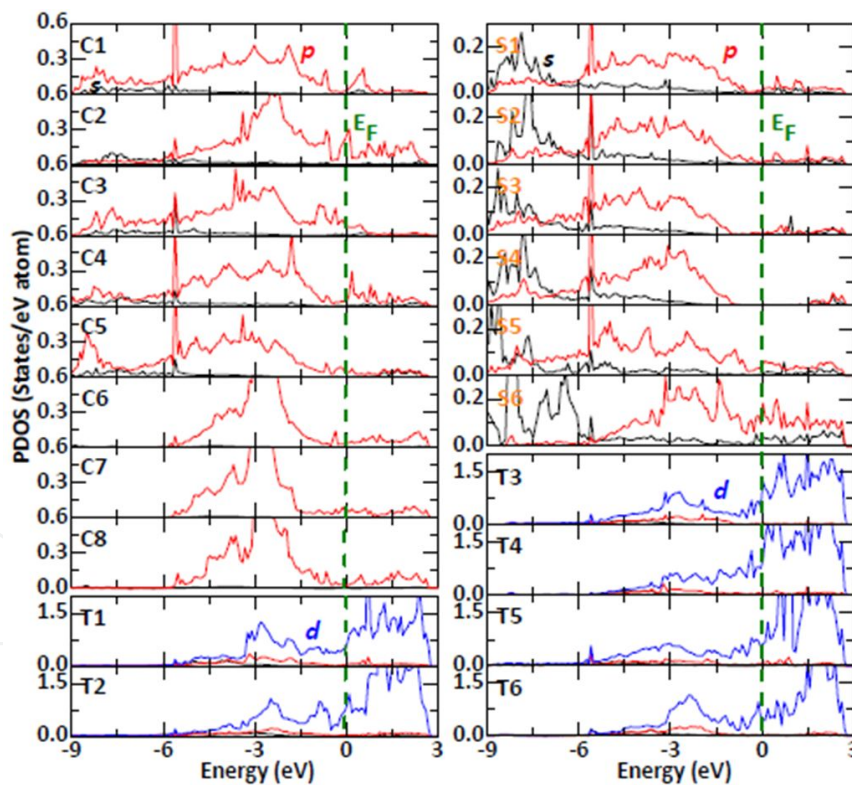


Figure 21. PDOS (states/eV atom) of several selected atoms at or far from the large terrace. Refer to Fig. 16(c) for the sites of the selected atoms [20].

The fully relaxed structure of the intermediate terrace is shown in Fig. 16(b), where one can see a Si-Si bonding at the hollow site (on two sides of the zigzag line). Figure 19 shows PDOS plot of several representative atoms on or near terrace (labeled in Fig. 16(b)), where

one can note that (i) gap states at E_F appear for the C (C2~C4) and Si (S1,S2) atoms in SiC near terrace, (ii) a hybridization is observed between the Ti d (Si p) and O p levels just below E_F , an indication of the formation of covalency, and (iii) the impact of terrace on the electronic states of both SiC and Ti_3SiC_2 is confined, as the PDOS returns to its bulk value for the atoms away from terrace (*e.g.*, C5, C8, S4, S6, T6). Interestingly, overall feature of the PDOS for either the C (C1~C4) or Si (S1~S3) atoms around terrace differs from one another, suggesting a strong effect of terrace on electronic states of both SiC and Ti_3SiC_2 .

Figure 20 shows contour plots of charge density and density difference for the relaxed intermediate terrace intersected along the same plane as in Fig. 18. Like what was seen in the small terrace, the majority of charges remain concentrated on C in two different ways: the charge distribution on the C in Ti_3SiC_2 (*e.g.*, C8) is of spherical symmetry, while that on the C in SiC (*e.g.*, C5) has notable lobes pointed toward their adjacent Si. However, some C atoms near terrace (indicated by arrows in Fig. 12(a)) have lobe and sphere outline simultaneously. Moreover, charges are distributed along the bonds near terrace (on two sides of zigzag line), which together with the charge localization on C atoms infers that the intermediate terrace has a mixed covalent and ionic bonding as well. Evidently, the charge gain on C is at expense of charge loss on their neighboring cations (Fig. 20(b)).

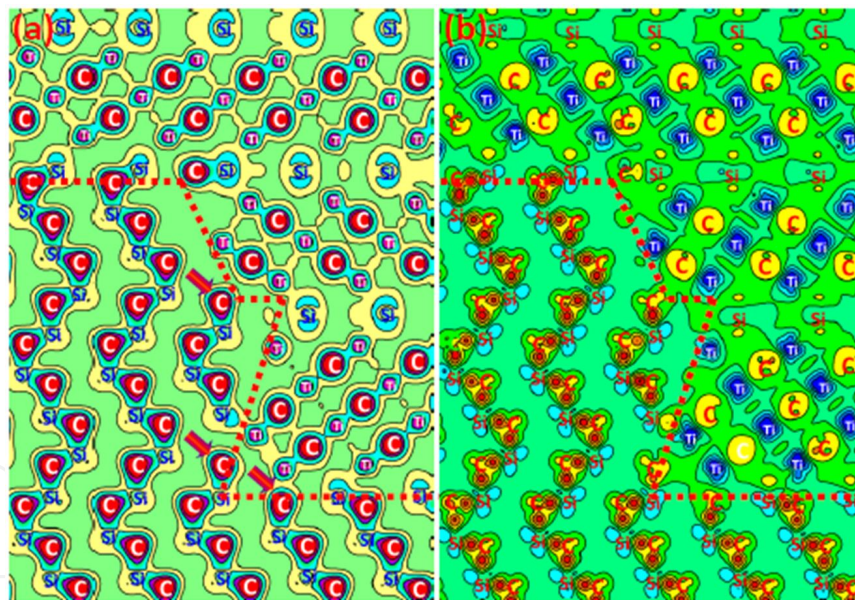


Figure 22. Contour plots of (a) charge density and (b) charge-density difference for the large terrace viewed along the (11-20) plane. The scale is the same as in Fig. 18. The site of terrace is indicated by a zigzag line and the atoms intersecting the contour plane are labeled [20].

Figure 16(c) illustrates optimized atomic geometry of the large terrace, where a Si-Si bonding is revealed. Figure 21 shows the PDOS of the large terrace, where one can notice that electronic structure is influenced remarkably by terrace. The key point is that there emerge notable peaks at E_F for both the C (C1~C5) and Si (S1~S3, S5, S6) surrounding terrace. However, such gap states are screened rapidly, since the atoms in SiC away from terrace (S4) show no peak at E_F at

all, which implies that the effect of terrace is confined to within a couple of layers. Moreover, a substantial hybridization is seen between the Ti d and Si (C) p levels below E_F , which indicates the formation of covalent bonding. The covalency is also reflected in the charge-density plot (Fig. 22(a)) showing lobes for the C in SiC and charge accumulation along the bonds in Ti_3SiC_2 . These, along with the charge distribution on C at expense of Ti and Si (Fig. 22(b)), indicate that bonding near terrace is again primarily ionic, yet maintains a certain degree of covalency. Finally, both the electron density and density difference for some atoms near terrace (indicated by arrows) deviate severely from those for their bulk counterparts, implying an essential electronic role of the Ti_3SiC_2 in the semiconductor.

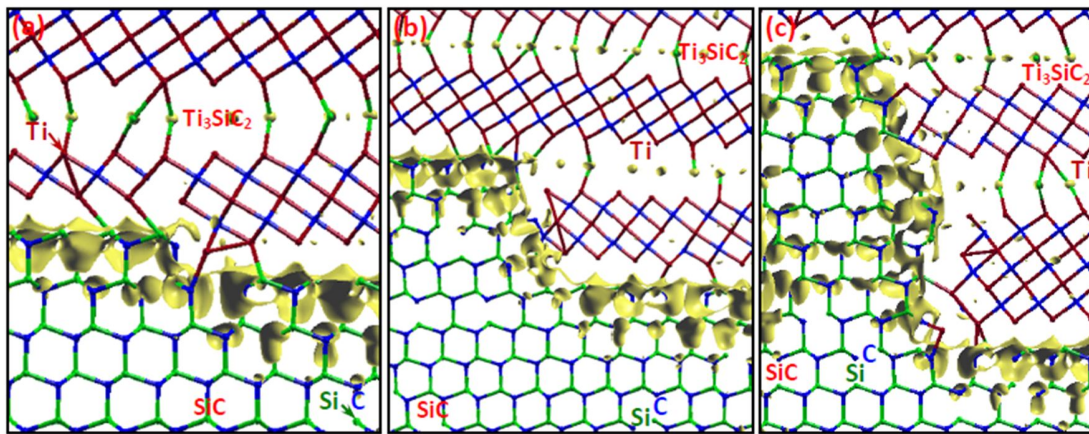


Figure 23. Isosurface plots for (a) small, (b) intermediate, and (c) large terrace along the (11-20) plane in an energy window ($E_F - 0.5$ eV, E_F). The charges on Ti_3SiC_2 are omitted for clarity [20].

4.3. Electron distribution near Fermi energy

Although the PDOS and charge analyses can reveal valuable information on the bonding nature near terrace, they provide limited insights into matters regarding electron distribution around E_F , which is strongly related to the electronic conduction over terrace. Figure 23 shows electron-density isosurface near E_F along the (11-20) plane for the three terraces. The electrons are accumulated substantially around all the terraces in a spatially connected fashion, which are extended as far as several atomic layers into SiC, regardless of dimension of the terraces. Such a broad electron distribution provides a likely electron conduction channel to allow current transport across a few layers of the semiconductor, which indicates that terraces could also be one of the origins underlying the observed ohmic nature in the metal/SiC contact system. One can also note that the three terraces are comparable in the amount of accumulated charge at E_F , inferring that the dimension of terrace plays an insignificant role in affecting electron transport across the contact. It is worthy of mentioning that the electron density at E_F is extremely high in Ti_3SiC_2 (sea of electrons, not shown for clarity), yet turns almost nil for the SiC atoms away from terrace, which can be understood on the fact that the Ti_3SiC_2 is intrinsically metallic, whereas the SiC is semiconducting.

5. Discussion and conclusions

The current understanding of formation origin of Ohmic contact, which is based mainly on experimental studies of property measurement and structure characterization, can be summarized in three main points [27-30]: (1) the deposited Al (80 at%) might diffuse in part into the SiC and dope heavily the semiconductor because Al is well-known to act as a *p*-type dopant for SiC, (2) the high density of pits, spikes, or dislocations may be generated underneath the contacts after annealing so that current can transport primarily through these defects due to the possible enhancement of electric field at these features and semiconductor doping at these locations, (3) formation of intermediate semiconductor layer between the deposited metals and semiconductor, which consists of silicides or carbides, could divide the high barrier height into lower ones, thus reducing the effective barrier height.

The findings presented first demonstrate that no Al is clearly segregated around the interfacial region, in particular at the top few layers of SiC, which rules out the possibility of additional Al doping. Though a small amount of residual Al is found to be present, mostly in a form of Al_4C_3 compound, it may locate on the surface of annealed contacts rather than in the layer directly contacted to the SiC, thus playing a negligible role in Ohmic contact formation. The majority of deposited Al is evaporated during annealing because of its low melting point and high equilibrium vapor pressure. The dominant role played by Al in the TiAl system is to assist the formation of liquid alloy so as to facilitate chemical reaction. Furthermore, careful characterization of the interfacial region reveals that the substrate and the generated compound are epitaxially oriented and well matched at interface with no clear evidence of high density of defects. This suggests that the morphology might not be the key to understanding the contact formation. In support of this speculation, it has been observed previously that Ti Ohmic contacts can be possibly generated without any pitting and that pit-free Ohmic contacts can be fabricated.

One remaining theory is the alloy-assisted Ohmic contact formation. This alloy is determined to be ternary Ti_3SiC_2 , which has also been corroborated by other experiments. Since the bulk Ti_3SiC_2 has already been found to be of metallic nature both in experiment and theory, the contact between Ti_3SiC_2 and its covered metals should show Ohmic character and thus the SiC/ Ti_3SiC_2 interface should play a significant role in Ohmic contact formation. This idea is supported by the fact that the determined interface has a lowered SBH due to the large dipole shift at interface induced by the partial ionicity and the considerable charge transfer. In addition, the interfacial states, as indicated by the electron distribution at E_F , are also viewed as a contributing factor in reducing the SBH. These states might be further enhanced by the possible presence of point defects at interface, although these structural defects have not been detected by the TEM study.

Interestingly, our calculations predict that an atomic layer of carbon emerges as the first monolayer of Ohmic contacts, which eventually affects interface electronic structure. Such trapped carbon was previously studied in both other interfacial systems theoretically by DFT and the TiNi Ohmic contacts on 4H-SiC experimentally by Auger electron spectroscopy. It was proposed that the carbon could be segregated to the interfacial area, strengthen-

ing interface substantially and reducing the Schottky barrier dramatically. Further, it was reported that the Ohmic contact can be realized by depositing carbon films only onto the SiC substrate, indicative of the determinative role of carbon in the Ohmic contact formation. The important role played by carbon in our study can be traced to the two interfacial Si layers, which provide possible sites for carbon segregation due to the strong Si-C interaction. However, direct imaging of the trapped carbon is still difficult in present study and further characterization requires the high-voltage EM and/or other advanced microscopic techniques.

We then demonstrate that atomic-scale Ti_3SiC_2 -like bilayer can be embedded in the SiC interior, forming an atomically ordered multilayer that exhibits an unexpected electronic state with the point Fermi surface, in stark absence in respective bulk constituents. The valence charge is found to be confined largely within the bilayer in a spatially connected way, which serves as a possible conducting channel to enhance the current flow over the semiconductor. Such a heterostructure with unusual properties is mechanically robust, rendering its patterning for technological applications likely. Finally, the atomic structures of terraces at the contacts in SiC devices are investigated and bridged to their electronic properties at an atomic scale. Experimentally, newly formed carbide Ti_3SiC_2 is demonstrated to bond directly to silicon carbide in the terrace region in an epitaxial and atomically ordered fashion, regardless of dimension of terraces. Further first-principles calculations reveal gap states in the semiconductor layers and a substantial charge accumulation around terraces in a connected and broadly distributed manner. The presence of gap states at Fermi energy and the likelihood to serve as electron conduction channels to allow current flow over the semiconductor identify the terraces as one of the origins underlying the ohmic contact in silicon carbide electronics. Such a combined experimental and theoretical investigation provides insight into the complex atomic and electronic structures of buried terraces, which should be applicable to addressing contact issues of interest in other electronic devices.

To summarize, we have determined in this chapter atomic-scale structures of Ohmic contacts on SiC and related them to their electronic structures and electric properties, aimed at understanding the formation mechanism of Ohmic contact in TiAl-based system. The combined HAADF-DFT study [31] represents an important advance in relating structures to device properties at an atomic scale and is not limited to the contacts in SiC electronics. Our results show that the main product generated by chemical reaction can be epitaxial and have atomic bonds to the substrate. The contact interface, which could trap an atomic layer of carbon, enables lowered Schottky barrier due to the large interfacial dipole shift associated with the considerable charge transfer. The atomic-scale Ti_3SiC_2 -like bilayer is embedded well in SiC bulk interior in an epitaxial, coherent and atomically abrupt manner, which exhibits an unexpected state with a point Fermi surface. Moreover, the formed Ti_3SiC_2 can even be epitaxial and atomically ordered on SiC substrate near terrace, which induces pronounced gap states at E_F in the semiconductor layers. Charges are accumulated heavily surrounding terrace in a spatially connected fashion, irrespective of dimension of the terraces, which suggests the possibility of terraces as likely electron conduction channels to allow current transport across the semiconductor. The inducing of gap states and the capability to enable current flow over the semiconductor identify the terraces as one of the origins underlying

the Ohmic nature in the metal/SiC contact system as well. These findings are relevant for technological improvement of contacts in SiC devices, and this chapter presents an important step towards addressing the current contact issues in wide-band-gap electronics.

Acknowledgements

The author acknowledges M. Saito, S. Tsukimoto, at the WPI Research Center, Advanced Institute for Materials Research, Tohoku University and Y. Ikuhara at the The University of Tokyo for their collaborations. The author thanks S. Watanabe at The University of Tokyo for allowing our use of computational resources. The present study was supported in part by a Grant-in-Aid for Scientific Research on Priority Area, "Atomic Scale Modification (474)" from the Ministry of Education, Culture, Sports, Science, and Technology of Japan. Z. W acknowledges financial supports from the Grant-in-Aid for Young Scientists (A) (Grant No. 24686069) and the Challenging Exploratory Research (Grant No. 24656376). The calculations were carried out on a parallel SR11000 supercomputer at the Institute for Solid State Physics, Univ. of Tokyo.

Author details

Zhongchang Wang*

Address all correspondence to: zawang@wpi-aimr.tohoku.ac.jp

WPI Research Center, Advanced Institute for Materials Research, Tohoku University, Japan

References

- [1] Perez-Wurfl, I., Krutsinger, R., Torvik, J. T., & Van Zeghbroeck, B. (2003). 4H-SiC Bipolar Junction Transistor with High Current and Power Density. *Solid State Electronics*, 47, 229-231.
- [2] Lee, S. K., Zetterling, C. M., Danielsson, E., Östling, M., Palmquist, J. P., Högberg, H., & Jansson, U. (2000). Electrical Characterization of TiC Ohmic Contacts to Aluminum Ion Implanted 4H-Silicon Carbide. *Applied Physics Letters*, 77, 1478-1480.
- [3] Pécz, B. (2001). Contact Formation in SiC Devices. *Applied Surface Science*, 184, 287-294.
- [4] Crofton, J., Barnes, P. A., & Williams, J. R. (1993). Contact Resistance Measurements on p-type 6H-SiC. *Applied Physics Letters*, 62, 384-386.

- [5] Mohney, S. E., Hull, B. A., Lin, J. Y., & Crofton, J. (2002). Morphological Study of the Al-Ti Ohmic Contact to p-type SiC. *Solid State Electronics*, 46, 689-693.
- [6] Nakatsuka, O., Takei, T., Koide, Y., & Murakami, M. (2002). Low Resistance TiAl Ohmic Contacts with Multi-Layered Structure for p-Type 4H-SiC. *Materials Transactions*, 43, 1684-1688.
- [7] Johnson, B. J., & Capano, M. A. (2004). Mechanism of Ohmic Behavior of Al/Ti Contacts to p-type 4H-SiC After Annealing. *Journal of Applied physics*, 95, 5616-5620.
- [8] Chang, S. C., Wang, S. J., Uang, K. M., & Liou, B. W. (2005). Investigation of Au/Ti/Al Ohmic Contact to N-type 4H-SiC. *Solid State Electronics*, 49, 1937-1941.
- [9] Ohyanagi, T., Onose, Y., & Watanabe, A. (2008). Ti/Ni Bilayer Ohmic Contact on 4H-SiC. *Journal of Vacuum Science and Technology B*, 26, 1395-1362.
- [10] Tsukimoto, S., Nitta, K., Sakai, T., Moriyama, M., & Murakami, M. (2004). Correlation Between the Electrical Properties and the Interfacial Microstructures of TiAl-Based Ohmic Contacts to p-type 4H-SiC. *Journal of Electronic Materials*, 33, 460-466.
- [11] Wang, Z. C., Tsukimoto, S., Saito, M., & Ikuhara, Y. (2009). SiC/Ti₃SiC₂ Interface: Atomic Structure, Energetics, and Bonding. *Physical Review B*, 79, 045318, 1-10.
- [12] Nellist, P. D., Chisholm, M. F., Dellby, N., Krivanek, O. L., Murfitt, M. F., Szilagy, Z. S., Lupini, A. R., Borisevich, A., Sides Jr, W. H., & Pennycook, S. J. (2004). Direct Sub-Angstrom Imaging of a Crystal Lattice. *Science*, 305, 1741.
- [13] Wang, Z. C., Saito, M., Mc Kenna, K. P., Gu, L., Tsukimoto, S., Shluger, A. L., & Ikuhara, Y. (2011). Atom-Resolved Imaging of Ordered Defect Superstructures at Individual Grain Boundaries. *Nature*, 479, 380-383.
- [14] Wang, Z. C., Tsukimoto, S., Saito, M., & Ikuhara, Y. (2009). Atomic and Electronic Structure of the YBa₂Cu₃O₇/SrTiO₃ Interface from First Principles. *Journal of Applied Physics*, 106, 093714-1-8.
- [15] Wang, Z. C., Tsukimoto, S., Saito, M., & Ikuhara, Y. (2009). Individual Charge-Trap-ping Dislocations in an Ionic Insulator. *Applied Physics Letters*, 95, 184101-1-3.
- [16] Wang, Z. C., Zeng, W., Gu, L., Saito, M., Tsukimoto, S., & Ikuhara, Y. (2010). Atomic-Scale Structure and Electronic Property of the LaAlO₃/TiO₂ Interface. *Journal of Applied Physics*, 108, 113701-1-9.
- [17] Wang, Z. C., Saito, M., Tsukimoto, S., & Ikuhara, Y. (2009). Interface Atomic-Scale Structure and its Impact on Quantum Electron Transport. *Advanced Materials*, 21, 4966-4969.
- [18] Wang, Z. C., Tsukimoto, S., Saito, M., Ito, K., Murakami, M., & Ikuhara, Y. (2009). Ohmic Contacts on Silicon Carbide: The First Monolayer and its Electronic Effect. *Physical Review B*, 80, 245303, 1-12.

- [19] Wang, Z. C., Tsukimoto, S., Sun, R., Saito, M., & Ikuhara, Y. (2011). Atomic-Scale Ti_3SiC_2 Bilayers Embedded in SiC: Formation of Point Fermi Surface. *Applied Physics Letters*, 98, 104101-1-3.
- [20] Wang, Z. C., Saito, M., Tsukimoto, S., & Ikuhara, Y. (2012). Terraces at Ohmic Contact in SiC Electronics: Structure and Electronic States. *Journal of Applied Physics*, 111, 113717-1-18.
- [21] Kresse, G., & Hafner, J. (1993). Ab initio Molecular Dynamics for Liquid Metals. *Physical Review B*, 47, 558-561.
- [22] Wang, X. G., Smith, J. R., & Evans, A. (2002). Fundamental Influence of C on Adhesion of the $\text{Al}_2\text{O}_3/\text{Al}$ Interface. *Physical Review Letters*, 89, 286102-1-4.
- [23] Wang, Z. C., Saito, M., Tsukimoto, S., & Ikuhara, Y. (2011). Heterointerfaces: Atomic Structures, Electronic States, and Related Properties. *Journal of the Ceramics Society of Japan*, 119, 783-793.
- [24] Pennycook, S. J., & Boatner, L. A. (1988). Chemically Sensitive Structure-Imaging with a Scanning Transmission Electron Microscope. *Nature*, 336, 565-567.
- [25] Ching, W. Y., Xu, Y. N., Rulis, P., & Ouyang, L. Z. (2006). The Electronic Structure and Spectroscopic Properties of 3C, 2H, 4H, 6H, 15R and 21R Polymorphs of SiC. *Materials Science and Engineering A*, 422, 147-156.
- [26] Wang, Z. C., Kadohira, T., Tada, T., & Watanabe, S. (2007). Nonequilibrium Quantum Transport Properties of a Silver Atomic Switch. *Nano Letters*, 7, 2688-2692.
- [27] Gao, M., Tsukimoto, S., Goss, S. H., Tumakha, S. P., Onishi, T., Murakami, M., & Brilison, L. J. (2007). Role of Interface Layers and Localized States in TiAl-Based Ohmic Contacts to p-Type 4H-SiC. *Journal of Electronic Materials*, 36, 277-284.
- [28] Tanimoto, S., Kiritani, N., Hoshi, M., & Okushi, H. (2002). Ohmic Contact Structure and Fabrication Process Applicable to Practical SiC Devices. *Materials Science Forum*, 389-393, 879-884.
- [29] Morkoc, H., Strite, S., Gao, G. B., Lin, M. E., Sverdlov, B., & Burns, M. (1994). Large-band-gap SiC, III-V Nitride, and II-VI ZnSe-based Semiconductor Device Technologies. *Journal of Applied physics*, 76, 1363-1398.
- [30] Lu, W., Mitchel, W. C., Thornton, CA, , W. E., Landis, G. R., & Smith, S. R. (2003). Ohmic Contact Behavior of Carbon Films on SiC. *Journal of the Electrochemical Society*, 153, G177-G182.
- [31] Wang, Z. C., Okude, M., Saito, M., Tsukimoto, S., Ohtomo, A., Tsukada, M., Kawasaki, M., & Ikuhara, Y. (2010). Dimensionality-Driven Insulator-Metal Transition in A-site Excess Non-stoichiometric Perovskites. *Nature Communications*, 1, 106.

